IOP Publishing Modelling and Simulation in Materials Science and Engineering

Modelling Simul. Mater. Sci. Eng. **23** (2015) 025010 (13pp) doi:10.1088/0965-0393/23/2/025010

Onset of ductility and brittleness in silicon nanowires mediated by dislocation nucleation

Firas Abed El Nabi, Julien Godet, Sandrine Brochard and Laurent Pizzagalli

Institut Pprime, Dept of Physics and Mechanics of Materials, UPR 3346 CNRS-University of Poitiers-SP2MI, BP 30179, 86962 Chasseneuil Futuroscope Cedex, France

E-mail: firas.abed.el.nabi@univ-poitiers.fr

Received 24 June 2014, revised 11 December 2014
Accepted for publication 23 December 2014
Published 22 January 2015

Abstract

Most studies show that materials at the nano-scale have different mechanical properties than in the bulk state. Semiconductors like silicon and germanium are brittle in the bulk state, but when their size is reduced to the nano-scale they appear to be ductile. Under tensile loading, we performed molecular dynamics simulations on silicon crystalline nanowires of different lengths. We present the details of the obtained mechanisms that led to ductility and brittleness. In the case of ductility, dislocation nucleation was observed with a signature of surface step formation on the surface and in the case of brittleness a cavity was formed after the distinct formation of a wedge-like shape on the surface. Interestingly, a common mechanism taking place behind ductility and brittleness is dislocation nucleation. We believe that the observed mechanisms reveal interesting information for understanding and explaining the size dependent brittle to ductile transition.

Keywords: molecular dynamics, semiconductor, ductile mechanisms, fracture mechanisms, plasticity, nanopillars

(Some figures may appear in colour only in the online journal)

1. Introduction

Due to their remarkable mechanical [1–3], electrical [4, 5] and optical properties [6–8], semiconductor nanowires (NWs) are increasingly used in a large variety of modern technology applications such as light emitting diodes [9] and for constructing nano-scale electronic devices like field effect transistors [5]. It is then important to fully characterize their properties.

Recent experimental advances allow us to push the investigation of semiconductor NWs to new limits. Hence, most studies show that materials at the nano-scale have different mechanical properties than in the bulk state. For example, an increase in the yield stress is observed in nano-objects compared to the bulk material, reaching in some cases the theoretical elasticity limit [3]. Furthermore, a brittle to ductile transition with size has been experimentally revealed for semiconductors [10, 11]. In fact, at room temperature semiconductors like silicon and germanium are brittle in the bulk state, but when their size is reduced to the nano-scale they appear to be ductile. Since brittleness can have in some applications catastrophic consequences leading to the failure of the device, understanding the brittle to ductile transition at small scale is highly desirable.

Various experimental, as well as numerical simulation studies, were conducted on silicon to understand the physics behind the size dependent brittle to ductile transition, by changing either the deformation axis ([1 1 0], [1 1 2] and [1 1 1]), the type of applied loading (compression, tension, bending) and the tested range of length and diameter. For example, using tensile tests, Han *et al* [1] showed that Si NWs oriented along the [1 1 0] axis are ductile below 60 nm while Zhu *et al* [12] showed that NWs are brittle for the same NW diameter but for different deformation axes ([1 1 2] and [1 1 1]). Bending tests were also performed by Tang *et al* [13] on Si NWs of diameters between 9 and 42 nm, and they showed that under compressive loadings NWs are ductile but that under tensile loadings NWs are brittle; their results were confirmed by molecular dynamics (MD) simulations.

In addition to the difference in the deformation rate, much higher in simulations than in experiments, NWs in experiments generally have larger diameters in comparison to NWs in simulations. Therefore it is quantitatively and qualitatively difficult to make straightforward comparisons. Still, indications of a transition with size can be noted in both simulations and experiments. Kang *et al* [14, 15] showed that for different temperatures, Si NWs of diameter below 4 nm are ductile, but they are brittle above this limit. Östlund *et al* [10] showed similar results in experiments but at higher diameters of about 310 nm.

Another potentially important parameter is the length of the NW. Indeed, in NWs, the onset of plasticity occurs at high strains, for which a significant amount of elastic energy is stored. Sudden release of this energy is expected to influence dislocation or crack propagation. Since the stored elastic energy is proportional to the length of the NW, the variation of the latter should be studied. Atomistic scale simulations are a particularly well suited tool for such investigations.

In this study, we present atomistic simulations done on Si NWs in order to have a better understanding of the brittle to ductile transition at the nano-scale. To elucidate the existence of such a transition, we performed multiple simulations on NWs of different length at a fixed diameter and for two temperatures. First, a presentation of the simulation details and parameters is given, followed by a description of the observed mechanisms. In the third part, we discuss the physics of the observed mechanisms and the results.

2. Simulation protocol

Figure 1 shows a typical NW used in our simulations, created by removing from bulk silicon all the atoms lying on the outside of a truncated cylinder oriented along the [0 1 1] direction. The length h and diameter d of the cylinder determine the geometry of the NW. The [0 1 1] orientation is chosen so that two possible slip planes, (1 1 1) and ($\bar{1}$ 1 1), can be activated. The Burgers vectors of the possible dislocations are $\frac{1}{2}$ [$\bar{1}$ 0 1] and $\frac{1}{2}$ [1 $\bar{1}$ 0] in (1 1 1) plane, and $\frac{1}{2}$ [1 1 0] and $\frac{1}{2}$ [1 0 1] in ($\bar{1}$ 1 1) plane. These four dislocations all have the same maximum

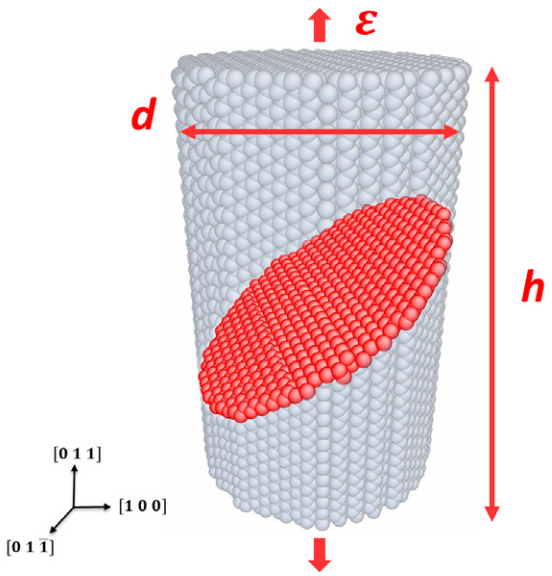

Figure 1. Typical NW used in our simulations. The glide plane ($\bar{1}$ 1 1) highlighted in red is one where most of the plastic activity is expected to take place. ε is the amount of strain applied on the NW. The atomic structure is visualized using AtomeEye [16].

Schmid factor (0.41). A dislocation with Burgers vectors $\frac{1}{2}$ [0 $\bar{1}$ 1] may also lie in both slip planes; however its Schmid factor is zero in both planes, so that it will never appear. We considered an orthorhombic simulation cell, with axis $\widehat{x} = [1\,0\,0]$, $\widehat{y} = [0\,1\,\bar{1}]$ and $\widehat{z} = [0\,1\,1]$, with periodic boundary conditions in all three directions and with a dimension along the $\widehat{z}$-axis chosen to be equal to the length h. Doing so removes artificial end effects and mimic an infinitely long NW. To avoid image interactions along the $\widehat{x}$- and $\widehat{y}$-axis, the size of the box is made large enough so that the distance between the NW and its periodic images is at least larger than twice the cut-off radius of the potential.

To be comparable in diameter size to the simulations done by Kang *et al* [14], we investigated the effect of increasing the NW length while keeping the diameter fixed at 7.7 nm, a value that showed consistent brittleness according to their work. Overall, NWs length spanned the range between 7.85 and 75.26 nm, which corresponds to a total number of atoms between 17 120 and 167 776 (table 1).

Interatomic interactions are described using a modified version of the Stillinger–Weber (SW) potential [17]. This version of the SW potential allows for a better description of defects, dislocation modeling, plastic properties of silicon and fracture description compared to the original formulation [18], while keeping the superior ability of the original potential for modeling silicon under high stress [19].

The LAMMPS simulation package [20] is used to perform classical MD at both 10 K and room temperature. For time integration in MD, we use the Verlet algorithm with a time step of 1 fs, tested to ensure energy convergence. The temperature is controlled with a Nosé–Hoover thermostat with a characteristic time for temperature fluctuation set to 150 fs. The initial velocities of all atoms are generated according to a Gaussian distribution corresponding to twice the equilibrium temperature.

Each run starts by imposing an initial strain of about 10% on the NW, thus remaining below the elastic limit (estimated from earlier simulations). The atomic structure is relaxed

Table 1. Aspect ratio, defined as the length h of the NW over its diameter d (fixed to 7.7 nm), the number of atoms as well as the number of tests for each simulated geometry.

h/d	h (nm)	Number of atoms	Number of simulations
1.02	7.85	17 120	10
1.53	11.78	25 680	15
2.75	21.17	46 224	10
4.08	31.41	68 480	10
10.01	75.26	167 776	5

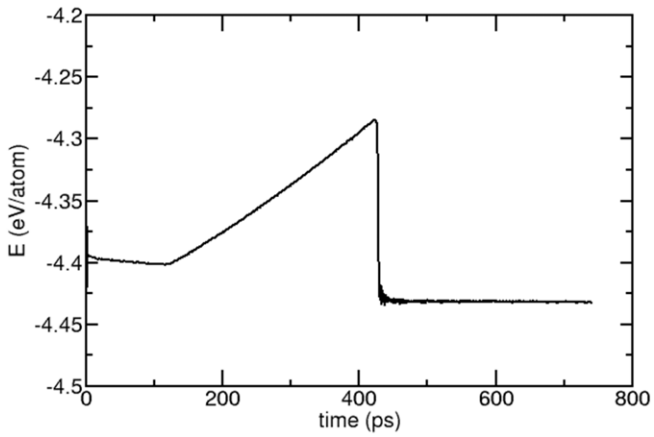

Figure 2. Monitoring the simulation with the energy graph. The abrupt drop on the energy curve, at about 430 ps, is a signature of a plasticity event.

to a local energy minimum by the conjugate gradient algorithm and equilibrated at a finite temperature for 100 ps. These first steps are essential, first to relax the NW with respect to Poisson's effect, second to promote surface reconstruction. It must be noted that the temperature for equilibration is that of the deformation test performed after, so the NW surfaces are most probably different for deformation tests performed at different temperatures. After equilibration, the tensile test is conducted in the NVT ensemble and NWs are elongated over 600 ps. A tensile strain is applied continuously by increasing the simulation box length and remapping all atoms coordinates to the new box at each time step to reach a final strain of 23%, a value estimated (from previous simulations) to be higher than the required strain to induce the first plasticity event. This corresponds to a strain rate of approximately 2×10^8 s^{-1}. During the whole procedure, the total energy is monitored, the first significant drop being a signature of plastic relaxation (see example in figure 2).

For every aspect ratio we repeated the simulation multiple times, changing at each run the random numbers generator seed for velocity distribution to ensure randomness. The purpose of these simulations is to acquire minimum statistics on the repeatability of identified plasticity mechanisms.

3. Description

A detailed analysis of the atomic structure was performed and we identified several plasticity mechanisms, ultimately leading to the rupture of the NW. In this section, we describe those

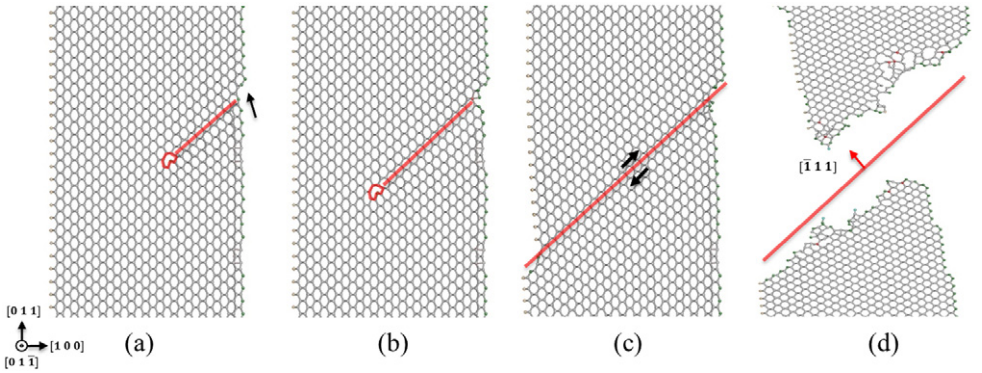

Figure 3. (*a*) Cross-section of a NW showing a non-dissociated perfect dislocation (60° dislocation core in red) gliding in a shuffle set plane (indicated in red) as well as the surface step left (black arrow) at the NW surface. (*b*) The nucleated dislocation propagates across the NW on a ($\bar{1}$ 1 1) plane, (*c*) a surface step is formed on the opposite surface where the dislocation emerges. (*d*) Under continuous tensile loading the NW ruptures along the ($\bar{1}$ 1 1) plane.

plasticity mechanisms regardless of the temperature and the size of the NW, discussed later in section 4.

For all tests the onset of plasticity is characterized by two distinct signatures on the surface of the NW, either a single step or a wedge. Step formation occurs when a dislocation half-loop is nucleated from the surface of the NW (figures 3(*a*) and (*b*)). For all the simulations described later on, the half-loop is a non-dissociated perfect dislocation with a 60° leading front located in a {1 1 1} plane of the 'shuffle' set, as expected from previous theoretical investigations [21–24]. This dislocation finally emerges at the opposite NW side, leaving another step. Following this initial event, several other similar dislocations are nucleated and glide on the same plane (figure 3(*c*)). Subsequently the two parts of the NW, above and below the glide plane, have been displaced in opposite directions. In this type of mechanism, slip occurs on a single plane throughout the tensile test. After multiple glide events, NWs rupture across the glide plane that has been activated (figure 3(*d*)).

Step formation was also obtained when multiple dislocations are nucleated at different surface locations (figure 4). Widely separated nucleation sites are activated, leading to dislocations gliding on parallel {1 1 1} planes (figures 4(*b*) and (*c*)). Subsequently, the same mechanism as for single glide takes place; dislocations propagate across the NW and create a shearing induced step on the other end where they emerge. Again, successive dislocations are nucleated and glide in the initially sheared planes. Eventually, under continuous tensile loading, multiple parts of the NW are shifted in opposite directions (figure 4(*d*)) until rupture occurs.

The second surface signature of the initial plasticity event is a localized wedge (figure 5), likely formed as a consequence of double gliding occurring on two intersecting dense planes, (1 1 1) and ($\bar{1}$ 1 1), suggesting that two glide systems were activated in the same region. A closer investigation of the NW structure shows that before a dislocation is nucleated (figure 5(*a*)), the atomic arrangement close to the surface is distorted (figures 5(*a*) and (*b*)). Such a distorted region may be formed by a random perturbation of the surface. Soon afterwards, a dislocation glides creating a step on the surface (figures 5(*b*) and (*c*)). The formation of a second surface step hints at the existence of another glide event taking place in a {1 1 1} plane (figure 5(*c*)).

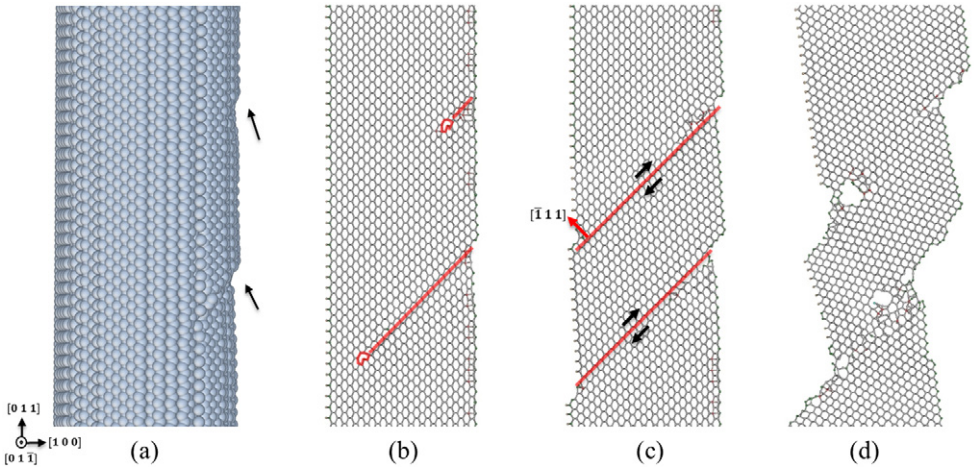

Figure 4. (*a*) Snapshot of a NW showing the formation of two steps on the surface due to two nucleation and glide events. Black arrows point to the surface steps. (*b*), (*c*) Perfect 60° dislocation cores gliding on ($\bar{1}$ 1 1) planes in the NW cross-section. Ultimately, the combined action of tensile loading and multiple dislocations propagating on the same plane breaks the atomic bonding and creates cavities (*d*) that will subsequently facilitate rupture on the ($\bar{1}$ 1 1) plane (not shown here).

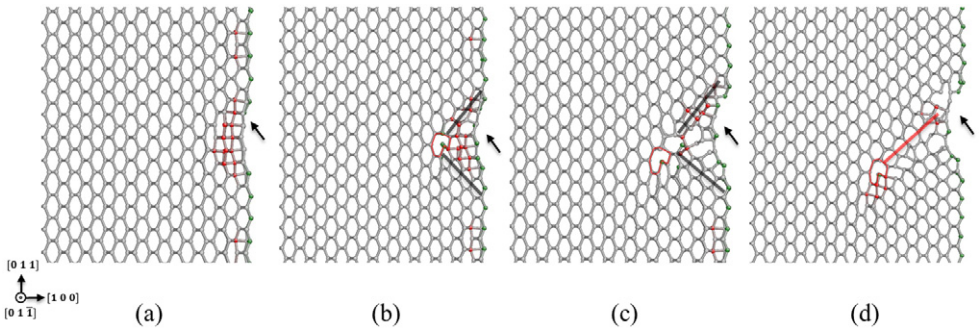

Figure 5. Wedge region formation (black arrow). (*a*) Over-coordination of atoms on the surface indicates an imminent plasticity event. (*b*) A dislocation is nucleated from the surface and glides in a (1 1 1) plane (dislocation core highlighted in red). A highly distorted region, confined between the two black lines (corresponding to (1 1 1) and ($\bar{1}$ 1 1) planes) and the surface, is also visible. (*c*) The two steps formed on the surface seem to correspond to the two glide events taking place on (1 1 1) and ($\bar{1}$ 1 1) planes; the former corresponds to the gliding of the surface nucleated dislocation in (1 1 1) plane, the latter is correlated to the existence of the distorted region. (*d*) In some cases, the surface nucleated dislocation glides further in the NW.

This second glide event is localized in a small region near the surface and it is difficult to precisely characterize it. The wedge-like shape thus formed on the surface becomes more pronounced as dislocations glide from the distorted region (figures 5(*c*), 6 and 7).

In the case of wedge formation, three subsequent scenarios were identified. In the first one, the wedge region acts as a dislocation nucleation center. Several dislocations half-loops are

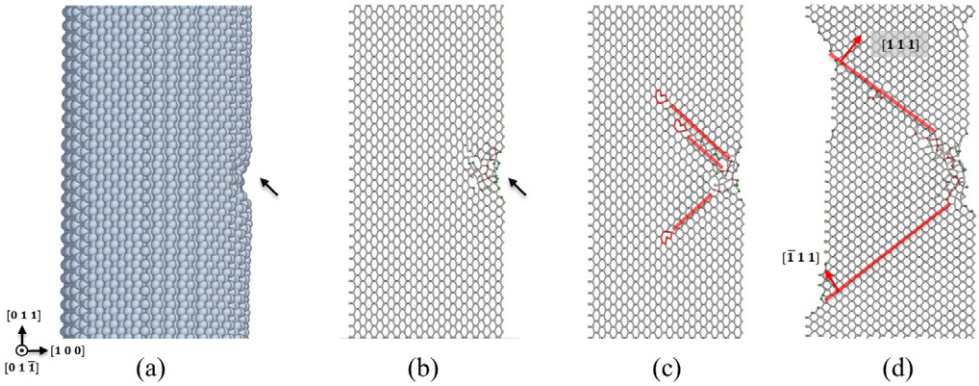

Figure 6. Wedge formation at the surface (*a*), resulting in a highly distorted region inside the NW (*b*). Several dislocations (60° dislocations core in red) are then nucleated from the wedge region (*c*) and glide on the activated planes (*d*). High dislocation activity leads to rupture after extensive shearing on the (1 1 1) plane (not shown here).

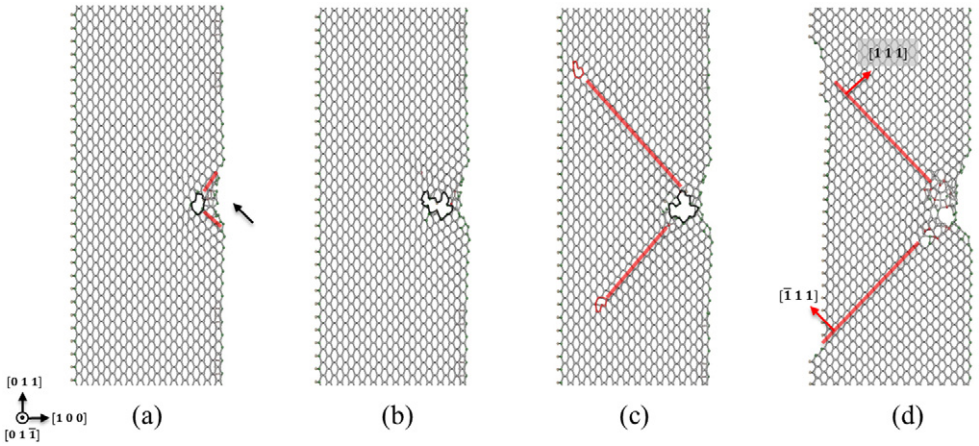

Figure 7. Cavity formation (displayed in black) in the distorted region following a wedge formation (*a*). The formed cavity can slightly expand along [1 0 0] and [0 1 $\bar{1}$], but remains confined inside the NW and connected to the wedge region (*b*). Then the cavity acts as a dislocation nucleation center, and a situation comparable to figure 6 is obtained (*c*), (*d*). Extensive glide on one of the planes leads to rupture (not shown) on that plane, in this case it is the ($\bar{1}$ 1 1) plane.

nucleated on (1 1 1) and ($\bar{1}$ 1 1) glide planes, intersecting in the wedge region (figures 6(*a*)–(*c*)). At the end the NW fails on one of these planes.

Another scenario leads to an additional cavity formation at the tip of the distorted region (figure 7(*a*)). This cavity has a limited extension in all three directions and remains connected to the wedge region. Dislocations are then nucleated at the cavity tip on both (1 1 1) and ($\bar{1}$ 1 1) planes (figures 7(*c*) and (*d*)), and eventually rupture will occur along the plane on which most of dislocation activity is taking place.

In the last scenario, the same cavity formation mechanism initially occurs. However in this case the cavity expands (figures 8(*b*)–(*d*)) along directions perpendicular to the NW

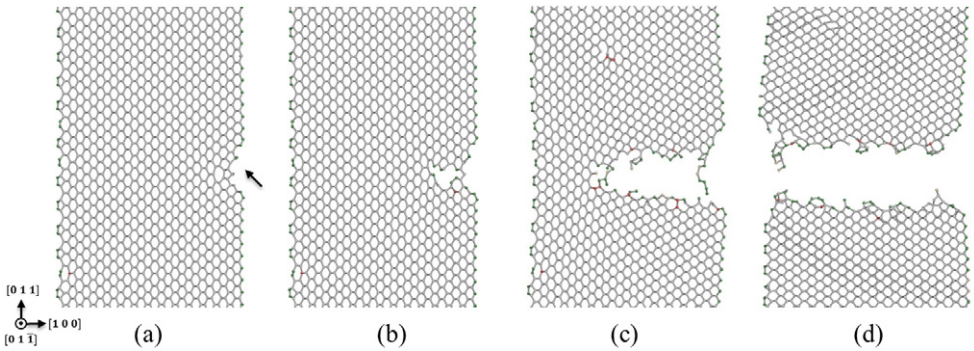

Figure 8. Wedge formation (*a*) followed by crack formation and propagation (*b*)–(*d*). A cavity is formed in the distorted region near the wedge (*b*), afterwards the cavity/crack expands (*c*) until complete fracture on the (0 1 1) plane (*d*).

axis until a crack forms and the NW fractures on the transverse (0 1 1) plane. During cavity expansion/crack propagation almost no dislocations were observed.

To summarize, we have seen that step/wedge formation was observed after dislocation nucleation. In the former case, one glide system was activated (figures 3 and 4). In the latter case, two glide events generate a wedge-like shape on the surface (figure 5), afterwards either the activation of two glide systems can take place (figures 6 and 7), or a cavity/crack formation and expansion can occur leading to fracture (figure 8).

4. Discussion

A comparison between the final states of the NWs, for the described events, leads to the conclusion that the NW rupture is ductile (i.e. shows a lot of dislocation activity) when a given mechanism involves rupture on one of the dense planes ($(\bar{1}\,1\,1)$ or $(1\,1\,1)$). This occurs for both one glide system activation (figures 3 and 4) and two glide systems activation (figures 6 and 7). On the other hand, the NW rupture is brittle when the mechanism leads to a fracture on the transverse plane, perpendicular to the deformation axis ((0 1 1) plane in our case).

However this classification (ductile or brittle), based on the final aspect of the NW after deformation, does not fully capture the true nature of scenarios depicted in figures 6 and 7. On the one hand, these processes share the same initial feature that nucleates the crack and leads to fracture as seen in figure 8, that is wedge formation. On the other hand, these processes exhibit ductility because of the final behavior of the NW, that is rupture due to extensive dislocation glide. For instance the case of figure 7 is a typical example of crack tip blunting [25] where the formed cavity plays the role of the crack tip. In the same manner, the mechanism seen in figure 6 can also be considered as a case of crack tip blunting where the crack tip is localized on the surface of the NW. Having these differences in mind, we can now classify our processes into three groups of behaviors: ductile (figures 3 and 4), intermediate (figures 6 and 7) and brittle (figure 8).

Table 2 shows the proportions of ductile, intermediate and brittle behaviors obtained at 10 and 300 K for all the tested aspect ratios. At 10 K, when the NWs aspect ratio increases, i.e. the length increases, the proportion of ductile events seems to slightly decrease while the proportion of brittle events seems to slightly increase.

At 300 K, increasing the NW length does not seem to alter the proportion of ductile events while the proportion of brittle events is close to zero for all aspect ratios. Comparing the total

Table 2. Proportion of identified ductile (D), intermediate (I) and brittle (B) behaviors, for different aspect ratios and temperatures.

	Temperature					
	10 K			300 K		
Ratio	D	I	B	D	I	B
1.02	0.7	0.3	0.0	1.0	0.0	0.0
1.53	0.8	0.2	0.0	1.0	0.0	0.0
2.75	0.5	0.3	0.2	0.8	0.1	0.1
4.08	0.6	0.2	0.2	1.0	0.0	0.0
10.01	0.6	0.2	0.2	1.0	0.0	0.0
Total	0.66	0.24	0.10	0.96	0.02	0.02

proportions for all aspect ratios at 10 K and room temperature leads to the following conclusion: increasing the temperature increases the number of ductile events and thus promotes the ductility, an expected result that is consistent with other studies [14, 22, 26]; intermediate and brittle behaviors are then less probable. We realized a few tests at 1 K that confirm this trend, since not a single ductile event (according to our classification) was observed for this very low temperature.

Looking at table 2, it appears that a larger variety of behaviors is obtained at 10 K, whereas the NWs are almost always ductile at 300 K. It can be explained as follows: in the light of our previous description of the shown mechanisms, the onset of plasticity is always mediated by dislocation nucleation. Therefore, the energy barrier associated with this first nucleation event can be expected to be the same for all three behaviors. Since the probability of thermal activation is low at 10 K, overcoming this energy barrier requires the application of a high stress, which in turn lowers the effect of differences in the activation energies of subsequent events. In addition, the large quantity of energy, due to high stress, released through dynamic relaxation allows the exploration of different configurations leading to a larger variety of plastic behaviors. On the contrary, at room temperature thermal activation is more efficient, therefore the required stress is smaller (figure 9) and there are less diverse cases. Note that for a given temperature and aspect ratio, the competition between the different plastic behaviors may be related to subtle surface effects, but the analysis of such effects is beyond the scope of the present work.

To end this part of the discussion, it is noteworthy to mention that the most noticeable size effects was seen when the aspect ratio of the NWs under study is above 2.75 for step formation and 1.53 for wedge formation. In fact, in cases of step formation, it was seen that for long NWs ($h/d \geqslant 2.75$), multiple step formation, as in figure 4, is more likely to take place; this is because more dislocation nucleation sites can be activated. As for the wedge formation, we found that when the NW aspect ratio is larger than 1.53, it is more likely to form a cavity in the wedge region (figure 7) and only when the NW aspect ratio is larger than 2.75, crack formation becomes possible. This suggests that for higher NW length, cavity formation would always be present after the wedge is formed and that there is a minimal length for crack formation and propagation to take place.

With the diameter $d = 7.7$ nm selected in this study, ductility was obtained in almost all the cases independently of the aspect ratio (in particular at 300 K), in contradiction with a numerical simulation study done by Kang *et al* [14]. According to the latter, a NW 7 nm in diameter and with an aspect ratio (h/d) of 10 is always brittle, apart for the highest temperature studied

(1200 K). The use of a different potential (MEAM) in this work than in ours, raises the critical issue of empirical potentials. It is difficult to estimate how much the results of atomistic studies, qualitatively and quantitatively, depend on the chosen potential. First-principles calculations would greatly improve this situation but they are, unfortunately, hardly feasible given the large number of atoms involved. Besides, experimentally, the size at which the size dependent brittle to ductile transition occurs decreases with the temperature; at 500 K, silicon pillars are ductile when their diameters are approximately below 1 μm [26], while at 300 K silicon pillars are ductile when their size is below 300 nm [10]. At 10 K we may then expect a much lower size for the transition. Despite the difference in the applied loading, tensile in our case, and taking into account the very large strain rates in simulations (compared to experiments), this could explain the observations of both brittle and ductile behaviors in our NWs of about 7 nm in diameter and 7–70 nm in length. Moreover, the deformation of these nano-objects at 300 K reveals in our study a ductile regime which is in agreement with the expected experimental behavior of nanopillars with dimensions below 300 nm.

Now we discuss the very first plasticity event feature, that is dislocation nucleation. This was a common aspect of ductile, intermediate and brittle behaviors. In fact, on the one hand, ductile events were mediated by dislocation nucleation on one or multiple parallel glide planes creating a step on the surface. On the other hand, intermediate and brittle events were initiated by dislocation nucleation inducing glide events on two intersecting planes creating a wedge on the surface. In both cases, the primary plasticity event was the nucleation of a dislocation. This suggests that a single mechanism could be at the origin of two completely different mechanical behaviors, brittleness and ductility. This also suggests that in a defect-free system (no pre-existing crack), crack nucleation would rely on the nucleation of dislocations. Our observations share some features with those made experimentally by Östlund *et al* [11], where a crack is nucleated at the intersection of two dislocations gliding in two different planes leading to fracture, with the main difference that in our study the two glide events occur in the close vicinity of each other.

Finally we turn to the analysis of the computed elasticity limit as a function of temperature and NWs aspect ratio (i.e. length). The elasticity limit is defined as the strain at which the first significant drop, associated to plastic deformation, is recorded on the energy curve. Since the onset of plasticity in all mechanisms is mediated by a dislocation nucleation, then the elasticity limit corresponds to the strain at which the first nucleation event takes place. Figure 9 shows this strain value averaged over all simulations, with respect to aspect ratio at 10 K and room temperature. The following remarks can be made: (i) as the aspect ratio increases the elasticity limit decreases, this behavior is seen at 10 K as well as at 300 K. This is because when the length of the NW increases, the number of possible dislocation nucleation sites increases as well. As a consequence, the probability of nucleation at a given strain increases, thus decreasing the elasticity limit [27]. A similar decrease was obtained in the case of nanowires terminated by fixed edges, to mimic clamping conditions. (ii) The elasticity limits recorded at 10 K are higher than those recorded at room temperature independently of the aspect ratio. This can be explained by the low thermal activation at 10 K, which reduces the probability of overcoming the energy barrier. Therefore, as already mentioned, the strain required to induce plasticity needs to be higher at 10 K than at room temperature; this result is consistent with previous studies [27, 28].

5. Conclusion

Molecular dynamics simulations of strained Si NWs of different lengths were performed using a modified version of the Stillinger–Weber potential. We identified several scenarios at the

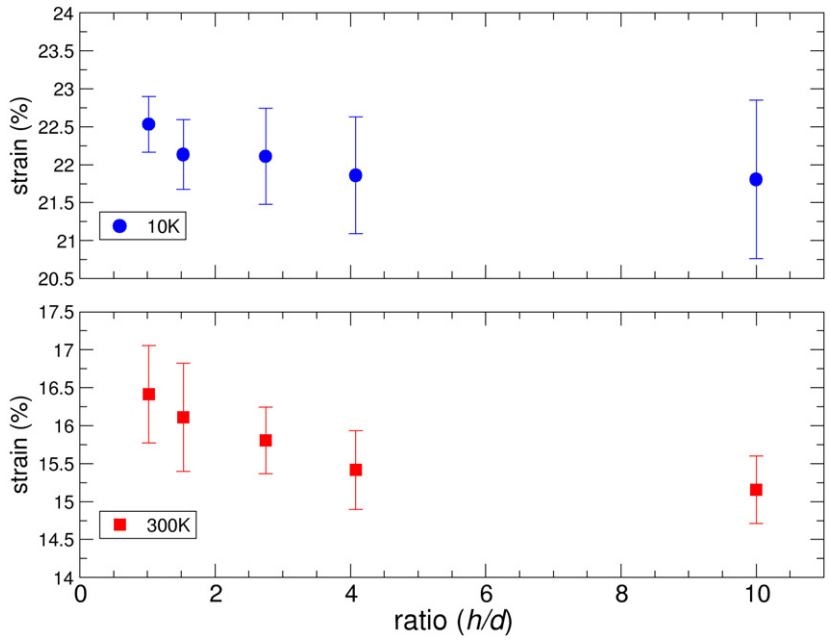

Figure 9. Graph showing the average elasticity limit calculated for each aspect ratio, at 10 K (up) and 300 K (down).

onset of plasticity: (i) surface dislocation nucleation and propagation, one glide system being activated; (ii) surface wedge formation acting as a crack tip, generating dislocations in two different glide systems; or fracture, by propagation of this crack tip.

As expected, the elasticity limit decreased with temperature. It also decreased with the NW length, that is explained by the increase of the number of dislocation nucleation sites (the first plasticity event being always dislocation nucleation). As for ductile, intermediate and brittle behaviors, it was found that NWs exhibit more ductility at room temperature than at 10 K. In addition, the length of the NW had a slight effect on its mechanical behavior at low temperature where brittleness was observed, whereas no significant effect at room temperature was noted and brittleness was almost never observed; the result at low temperature suggests that a minimal length for NWs is required in order to form a crack prior to fracture. Although our results showed a dominant ductile behavior at room temperature, which is in agreement with experimental studies, the existence of both brittle and ductile behavior at 10 K indicates that the transition size may be shifted at low temperatures as suggested by the trend of the experimental results.

Finally dislocation nucleation was observed when both ductile and brittle behaviors where initiated, which hints that cracks could be dislocation induced defects in pristine NWs.

Acknowledgments

We wish to thank 'l'Agence Nationale de la Recherche' for the financial support for this research under the grant reference ANR-12-BS04-0003-01. This work pertains to the French Government program 'Investissements d'Avenir' (LABEX INTERACTIFS, reference ANR-11-LABX-0017-01).

References

[1] Han X D, Zheng K, Zhang Y F, Zhang X N, Zhang Z and Wang Z L 2007 Low-temperature *in situ* large-strain plasticity of silicon nanowires *Adv. Mater.* **19** 2112–18

[2] Hoffmann S, Utke I, Moser B, Michler J, Christiansen S H, Schmidt V, Senz S, Werner P, Gösele U and Ballif C 2006 Measurement of the bending strength of vapor–liquid–solid grown silicon nanowires *Nano Lett.* **6** 622–5

[3] Kizuka T, Takatani Y, Asaka K and Yoshizaki R 2005 Measurements of the atomistic mechanics of single crystalline silicon wires of nanometer width *Phys. Rev.* B **72** 035333

[4] Chan C K, Peng H, Liu G, McIlwrath K, Zhang X F, Huggins R A and Cui Y 2008 High-performance lithium battery anodes using silicon nanowires *Nature Nanotechnol.* **3** 31–5

[5] Cui Y, Zhong Z, Wang D, Wang W U and Lieber C M 2003 High performance silicon nanowire field effect transistors *Nano Lett.* **3** 149–52

[6] Yang P 2005 The chemistry and physics of semiconductor nanowires *MRS Bull.* **30** 85–91

[7] Lieber C M 2011 Semiconductor nanowires: a platform for nanoscience and nanotechnology *MRS Bull.* **36** 1052–63

[8] Lieber C M and Wang Z L 2007 Functional nanowires *MRS Bull.* **32** 99–108

[9] Huang Y, Duan X and Lieber C M 2005 Nanowires for integrated multicolor nanophotonics *Small* **1** 142–7

[10] Östlund F, Rzepiejewska-Malyska K, Leifer K, Hale L M, Tang Y, Ballarini R, Gerberich W W and Michler J 2009 Brittle-to-ductile transition in uniaxial compression of silicon pillars at room temperature *Adv. Funct. Mater.* **19** 2439–44

[11] Östlund F, Howie P R, Ghisleni R, Korte S, Leifer K, Clegg W J and Michler J 2011 Ductile–brittle transition in micropillar compression of GaAs at room temperature *Phil. Mag.* **91** 1190–9

[12] Zhu Y, Xu F, Qin Q, Fung W Y and Lu W 2009 Mechanical properties of vapor–liquid–solid synthesized silicon nanowires *Nano Lett.* **9** 3934–9 pMID: 19691288

[13] Tang D-M, Ren C-L, Wang M-S, Wei X, Kawamoto N, Liu C, Bando Y, Mitome M, Fukata N and Golberg D 2012 Mechanical properties of Si nanowires as revealed by *in situ* transmission electron microscopy and molecular dynamics simulations *Nano Lett.* **12** 1898–904

[14] Kang K and Cai W 2010 Size and temperature effects on the fracture mechanisms of silicon nanowires: molecular dynamics simulations *Int. J. Plast.* **26** 1387–401 (special issue in honor of David L McDowell)

[15] Kang K and Cai W 2007 Brittle and ductile fracture of semiconductor nanowires—molecular dynamics simulations *Phil. Mag.* **87** 2169–89

[16] Li J 2003 Atomeye: an efficient atomistic configuration viewer, *Modelling Simul. Mater. Sci. Eng.* **11** 173–7

[17] Pizzagalli L, Godet J, Guénolé J, Brochard S, Holmstrom E, Nordlund K and Albaret T 2013 A new parametrization of the Stillinger–Weber potential for an improved description of defects and plasticity of silicon *J. Phys.: Condens. Matter* **25** 055801

[18] Stillinger F H and Weber T A 1985 Computer simulation of local order in condensed phases of silicon *Phys. Rev.* B **31** 5262–71

[19] Godet J, Pizzagalli L, Brochard S and Beauchamp P 2003 Comparison between classical potentials and *ab initio* methods for silicon under large shear *J. Phys.: Condens. Matter* **15** 6943 http://stacks.iop.org/0953-8984/15/i=41/a=004

[20] Plimpton S 1995 Fast parallel algorithms for short-range molecular dynamics *J. Comput. Phys.* **117** 1–19

[21] Guénolé J, Godet J and Brochard S 2011 Deformation of silicon nanowires studied by molecular dynamics simulations *Modelling Simul. Mater. Sci. Eng.* **19** 074003

[22] Godet J, Pizzagalli L, Brochard S and Beauchamp P 2004 Theoretical study of dislocation nucleation from simple surface defects in semiconductors *Phys. Rev.* B **70** 054109

[23] Godet J, Brochard S, Pizzagalli L, Beauchamp P and Soler J M 2006 Dislocation formation from a surface step in semiconductors: an *ab Initio* study *Phys. Rev.* B **73** 092105

[24] Pizzagalli L, Godet J and Brochard S 2009 Glissile dislocations with transient cores in silicon *Phys. Rev. Lett.* **103** 065505
[25] Thaulow C, Sen D and Buehler M J 2011 Atomistic study of the effect of crack tip ledges on the nucleation of dislocations in silicon single crystals at elevated temperature *Mater. Sci. Eng.* A **528** 4357–64
[26] Rabier J, Montagne A, Wheeler J M, Demenet J, Michler J and Ghisleni R 2013 Silicon micropillars: high stress plasticity *Phys. Status Solidi* **10** 11–5
[27] Zhu T, Li J, Samanta A, Leach A and Gall K 2008 Temperature and strain-rate dependence of surface dislocation nucleation *Phys. Rev. Lett.* **100** 025502
[28] Brochard S, Hirel P, Pizzagalli L and Godet J 2010 Elastic limit for surface step dislocation nucleation in face-centered cubic metals: temperature and step height dependence *Acta Mater.* **58** 4182–90